Elastocaloric effect of shape memory polymers in elastic response regime

Journal of Physics: Energy

PAPER

Elastocaloric effect of shape memory polymers in elastic response regime

Takamasa Hirai[1,*], Koichiro Uto[2,*], Mitsuhiro Ebara[2] and Ken-ichi Uchida[1]

[1] Research Center for Magnetic and Spintronic Materials, National Institute for Materials Science, Tsukuba 305-0047, Japan
[2] Research Center for Functional Materials, National Institute for Materials Science, Tsukuba 305-0044, Japan
* Authors to whom any correspondence should be addressed.

E-mail: HIRAI.Takamasa@nims.go.jp and UTO.Koichiro@nims.go.jp

Keywords: elastocaloric effect, shape memory polymer, elastic deformation, cross-linking, lock-in thermography

OPEN ACCESS

RECEIVED
30 January 2023

REVISED
29 June 2023

ACCEPTED FOR PUBLICATION
17 July 2023

PUBLISHED
27 July 2023

Abstract

Solid-state cooling/heating technology based on the elastocaloric effect is one of the promising alternatives to vapor compression systems. Large elastocaloric temperature modulation is often generated through the non-linear strain-induced structural transition by applying large strain and/or stress to ferroelastic materials. Recently, an unconventional approach to expand the application possibilities of the elastocaloric effect was demonstrated by processing elastocaloric materials into kirigami structures, which was inspired by the art of paper cutting. Using this approach, only a small stretch of processed conventional plastics can locally provide more efficient performance of elastocaloric temperature modulation than that of ferroelastic materials. To further improve such a unique functionality, it is necessary to find plastic or polymeric materials showing large elastocaloric effects in the linear elastic response regime that can be driven by a MPa-order weak stress application, where the non-linear structural transition is irrelevant. In this work, by means of a recently developed measurement technique for the elastocaloric effect based on the lock-in thermography, we found that shape memory polymers (SMPs) show prominent performance for elastocaloric temperature modulation that is larger than conventional plastics. SMPs enable the control of crystallinity by changing the cross-linking agents, melting temperature by changing the degree of polymerization, and orientation of the polymer chain segment by the shape memory effect. By utilizing the unique properties of SMPs, we manipulated their elastocaloric performance. The experimental results reported here will highlight the potential of smart polymers for flexible and durable elastocaloric applications.

1. Introduction

Demand for developing thermal management technologies is rapidly increasing with the remarkable increase in the number of electronic devices and in the amount of global energy use. Recently, for realizing an environment-friendly temperature control, a solid-state temperature modulation based on caloric effects has attracted large interests as a promising alternative to widely used vapor compression systems that employ greenhouse-gas refrigerants [1]. The caloric effects are characterized by an adiabatic temperature change ΔT_{ad} and/or an isothermal entropy change ΔS_{iso} in a solid via the application and removal of an external field, such as a magnetic field for the magnetocaloric effect [2, 3], an electric field for the electrocaloric effect [4], a hydrostatic pressure for the barocaloric effect [5] and a strain/stress for the elastocaloric effect [6, 7]. Among them, it is predicted that the temperature modulation based on the elastocaloric effect could be more efficient than other caloric effects and other solid-state temperature modulation technologies (e.g., thermoelectric effects) [7, 8]. To realize these advantages, extensive efforts have been exerted for developing practical applications and exploring materials for the elastocaloric effect.

A general formula of ΔT_{ad} and ΔS_{iso} for the elastocaloric effect is described as

$$\Delta T_{ad} = -\frac{T_0}{\rho c_p}\int_0^{\sigma}\left(\frac{\partial \varepsilon}{\partial T}\right)_{\sigma} d\sigma = -\frac{T_0 \Delta S_{iso}}{c_p}, \quad (1)$$

where T_0, ρ, c_p, and ε are the base temperature, density, specific heat, and uniaxial strain, respectively, and equation (1) is compromised by assuming that the value of c_p does not depend on T and σ [1]. Equation (1) shows that materials with large strain-induced ΔS_{iso} can have large cooling and heating capability. In general, the mechanism of strain-induced ΔS_{iso} is divided into three factors: (i) linear elastic deformation, (ii) non-linear structural transition, and (iii) atomic/molecular rearrangement, rotation, and/or deformation. The ΔS_{iso} contribution induced by (i) can be obtained in all solids within the range of the linear and reversible relationships between the stress σ and ε, where the magnitude of ΔT_{ad} is proportional to σ [9]. The mechanism (ii) corresponds to the strain-induced martensitic, ferroelastic, or glass transition, resulting in the drastically large ΔS_{iso}, which is usually much larger than ΔS_{iso} due to the mechanisms (i) and (iii). The mechanism (iii) includes a variety of effects, such as the nano-scale atomic reordering after structural transition [10], electric polarization reordering by the piezoelectric effect [11], and rubber-like entropy elasticity observed in an elastomer [12]. In elastocaloric materials, shape memory alloys (SMAs), such as NiTi-based alloys [13–16] and Cu-based alloys [17–19], are most promising owing to the contribution coming from the mechanism (ii). By using SMAs, the temperature modulation over 10 K has been achieved [13–16]. However, in such materials, the repetitive application of the large input stress of >0.5 GPa during the thermodynamic and mechanical cycles is required to drive the structural phase transition, which leads to device performance degradation due to irreversible plastic deformation, microcracks, and hysteresis energy loss [11, 15, 20, 21]. The natural rubber also shows the large elastocaloric temperature change due to strain-induced crystallization [22, 23], but at least several hundred percent change of ε is required to generate a temperature change comparable to SMAs [12, 24], which restricts the miniaturization of systems.

Recently, a different approach to manipulate the magnitude and distribution of the elastocaloric temperature change has been proposed and demonstrated based on the 'kirigami' processing, inspired by the art of paper cutting [25]. A programmable cutting pattern on a solid sheet artificially introduces a non-uniform spatial distribution of the internal stress against the application of uniaxial strain, generating focused elastocaloric heating and cooling sources at designed positions. In addition, the kirigami pattern gives ultrahigh stretchability and flexibility to solids, which can dramatically reduce the required stress for stretching. By processing the kirigami pattern on a polystyrene (PS) sheet, one of the conventional plastics, the performance of elastocaloric cooling/heating can locally exceed the values in previous reports using SMAs even though the applied strain (stress) is a few percents (a few MPa), where the dominant contribution of the elastocaloric effect of PS is the mechanism (i) without the glass transition. Despite the small ΔT_{ad} in conventional polymers, such a unique functionality driven a by MPa-order weak stress without hysteresis energy loss during mechanical cycles will open up unconventional applications for locally selective, flexible, and durable temperature modulators based on the elastocaloric effect and may utilize omnipresent mechanical energy that is currently wasted. To improve the perspective of elastocaloric kirigami temperature modulators, it is important to uncover materials with large elastocaloric performance in the region of elastic deformation because, in that region, the performance at a focused cooling/heating source in a kirigami-patterned sheet directly depends on the performance in the unpatterned sheet. Note that the magnitude of the elastocaloric temperature modulation normalized by the stress in the unpatterned PS sheet is $\sim 1.5 \times 10^{-8}$ K Pa^{-1}, which realizes the local temperature change of 0.4 K at typical positions by applying uniaxial strain (stress) of 1.0% (4.0 MPa) in the kirigami-patterned PS sheet [25].

In this study, we have investigated the elastocaloric effect in the region of reversible elastic deformation using unpatterned shape memory polymer (SMP) sheets (figure 1). SMPs, a group of a *smart* polymer, are cheaper, more flexible, and easier to be manufactured and processed than SMAs [26], so that SMPs are of significance in flexible/wearable electronics [27] and biomedical research fields [28]. Recently, the elastocaloric effect arising from the mechanism (ii) in an SMP has been reported [29], but the effect in the linear elastic response regime with small strain and stress has not been investigated yet. Although there are many SMPs, in this work, we used SMPs composed of poly(ε-caprolactone), one of the conventional semicrystalline SMPs [30, 31]. Hereafter, poly(ε-caprolactone) is abbreviated as PCL. By precisely designing the nanoarchitectonics of PCL, such as the number of branches and chain length, various physical properties, such as thermal, mechanical, and even shape memory properties, can be tuned [31–33]. We found that the performance of elastocaloric temperature change in PCL-based SMPs is larger than that in other conventional plastics. By changing the cross-linking agent and/or the degree of polymerization of PCL, the elastocaloric performance can be further enhanced; the maximum performance obtained here is twice as large as that in PS. In addition, we found that the performance of SMPs can also be improved by using the

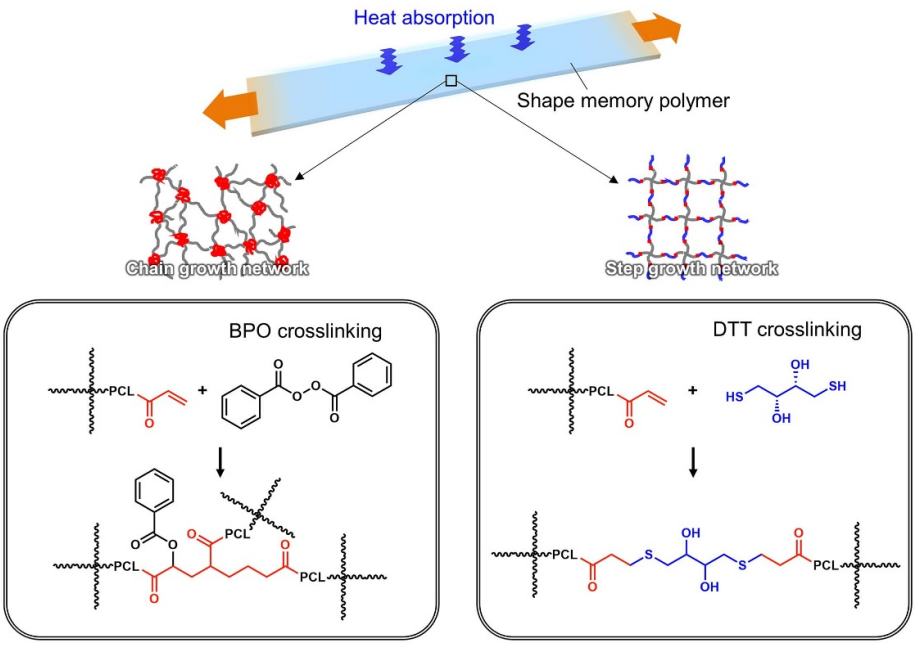

Figure 1. Schematic of the elastocaloric effect in tetra-branched poly(ε-caprolactone) (PCL)-based shape memory polymers (SMPs) crosslinked by benzoyl peroxide (BPO) or dithiothreitol (DTT), where the structural formulae of two SMPs are also shown.

shape memory effect, a unique characteristic of SMP, where the shape of SMP can be easily changed and fixed. The thermal management functionalities of SMPs and the systematic dataset will boost both basic and application studies in the communities of not only the caloric effects but also smart polymers.

2. Materials and methods

2.1. Sample preparation

Tetra-branched (4b) PCL was synthesized by ring opening polymerization of ε-caprolactone (CL) with the tetravalent initiator, pentaerythritol [31, 34]. The PCL with various degrees of polymerization ($x = 10$–70) (abbreviated as 4b*x*PCL) was designed by adjusting the ratio of pentaerythritol to CL during the polymerization. Thereafter, hydroxyl end groups of 4b*x*PCL were modified using acryloyl chloride to introduce polymerizable acrylate groups onto the branch ends. The 4b*x*PCL modified with acrylate groups were cross-linked by thermal polymerization with benzoyl peroxide (BPO) and Michael addition reaction with dithiothreitol (DTT) (figure 1). The acrylated 4b*x*PCL was dissolved at 45 wt.% in xylene containing 2-fold molar excess BPO to the end-group of the polymer. The solution was injected between glass slides with a ∼0.2 mm thick Teflon spacer. Subsequent thermal polymerization was conducted at 353 K for 16 h to obtain the cross-linked 4b*x*PCL (4b*x*PCL-BPO). In cross-linking with DTT, *N*,*N*-dimethylformamide was used as a solvent instead of xylene, and a solution was prepared by adding 0.5-fold molar amount of DTT against end-groups of polymer and a catalytic amount of triethylamine, and cross-linked 4b*x*PCL (4b*x*PCL-DTT) was obtained in the same manner as described above. The actual values of x were estimated at $x = 11$, 21, 32, 52, and 67 ($x = 11$, 21, 32, and 52) for 4b*x*PCL-BPO (4b*x*PCL-DTT) sheets by proton nuclear magnetic resonance spectroscopy. The thickness t of the 4b*x*PCL-BPO and -DTT samples is in the range of 0.1–0.2 mm. After fabrication, all the 4b*x*PCL SMP sheets are cut out into a strip with the width w of 6 mm. For comparison, we prepared five commercial plastic sheets: PS, polypropylene, polyvinyl-chloride, high density polyethylene (HDPE), and polyethylene-terephthalate with $t = 1.0$ mm and $w = 6$ mm, which are available from NaRiKa Corp., Japan. For the lock-in thermography (LIT) measurements (see section 2.3), the surface of the samples was coated with insulating black ink with an emissivity of >0.94 (JSC-3, JAPANSENSOR Corporation) to endure high and uniform thermal radiation.

2.2. Differential scanning calorimetry

The crystallinity ratio X_c and the melting temperature T_m, corresponding to the crystal-amorphous transition of SMPs, of the 4b*x*PCL-BPO and -DTT samples were estimated using the differential scanning calorimetry (DSC). All samples were first equilibrated at 353 K and then cooled to 253 K, followed by performing the measurements during the heating process to 353 K at a rate of 5 K min^{-1} under nitrogen

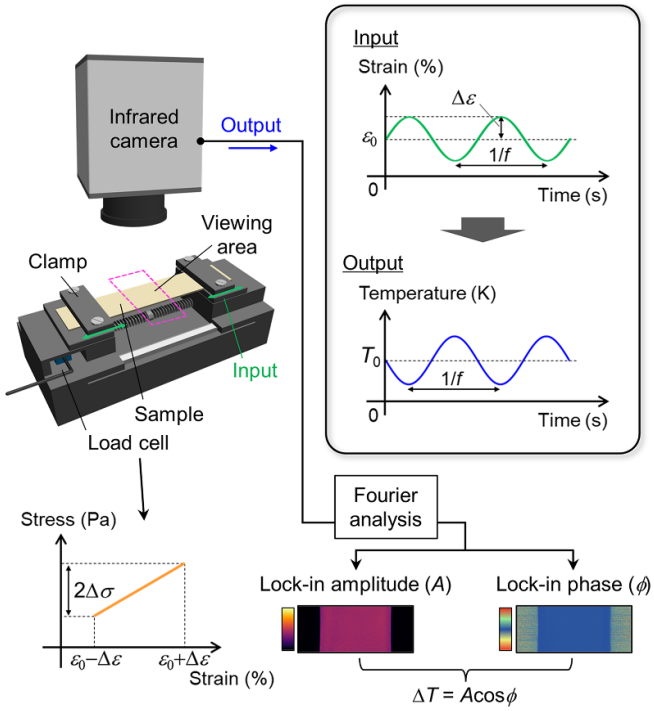

Figure 2. Measurement of the elastocaloric effect based on the lock-in thermography (LIT). By applying a sinusoidal-waved strain with the amplitude $\Delta\varepsilon$, offset ε_0, and frequency f, the sample temperature is sinusoidally modulated from the base temperature T_0 with the same f by the elastocaloric effect. Captured thermal images are transformed into lock-in amplitude (A) and phase (ϕ) images. During the LIT measurements, the $\Delta\sigma$-$\Delta\varepsilon$ curve is measured using the load cell.

atmosphere. The value of X_c was calculated from the enthalpy change quantified by DSC thermograms and the melting enthalpy of 100% crystalline PCL and that of T_m was defined as the temperature at the peak top of DSC thermograms [35, 36]. To check the reproducibility and estimate the magnitude of errors, the DSC measurements were conducted three times for each sample.

2.3. LIT measurement of elastocaloric effect

The temperature modulation generated by the elastocaloric effect was measured using the LIT technique [37]. In the LIT measurement, we recorded thermal images of a sample surface by applying a periodic oscillation of the input signal using an infrared camera and extracted a temperature change oscillating with the same frequency f as the input frequency [25, 38–42] (figure 2). Since the LIT method enables contact-free temperature measurements with high temperature and spatial resolutions and separation of the temperature change due to a target effect and a background signal, it is suitable to measure the elastocaloric temperature change in the small strain regime, compared with other methods for measuring the caloric effects [39]. The procedure of the LIT measurement for this study is as follows (see also figure 2). First, the samples were clamped at the distance $L_0 = 15$ mm on a motor-driven tensile machine with a load cell and a linear encoder, where the center between the two clamps was adjusted to the center of the viewing area of the infrared camera by using a custom-made ball screw. Second, a sinusoidal strain with the amplitude $\Delta\varepsilon$, offset ε_0, and $f = 1$ Hz was applied to the sample along its longitudinal direction, where $\Delta\varepsilon = \Delta l/L_0$ and $\varepsilon_0 = \Delta\varepsilon + 0.5\%$ with Δl being the amplitude of the sinusoidal elongation. Finally, the thermal images recorded were transformed into the lock-in amplitude A (>0) and phase ϕ ($0° \leqslant \phi < 360°$) images through Fourier analysis, in which A informs the magnitude of the elastocaloric temperature modulation and ϕ the sign of the temperature modulation as well as the time delay due to the thermal diffusion. In previous study, it was shown that the value of ϕ due to the elastocaloric effect in unpatterned plastic sheets at 1 Hz is nearly 180° and the contribution of thermal diffusion is negligible [25]. Unless otherwise specified, the integration time of each LIT measurement t_{int} is 60 s. The performance of the elastocaloric temperature modulation was thus quantified by $|\Delta T|/\Delta\sigma$, where ΔT is the elastocaloric temperature change calculated as $\Delta T = A\cos\phi$ and $\Delta\sigma$ is the stress for stretching the sample, calculated as $\Delta\sigma = \Delta F/wt$ with ΔF being the change in the load monitored using the load cell. All the LIT measurements were conducted at room temperature and under air atmosphere.

3. Results and discussion

3.1. Crystallinity and melting temperature of 4bxPCL SMPs

Figures 3(a) and (b) show the x dependence of X_c (T_m) for 4bxPCL-BPO and -DTT samples. In both SMPs, the decreasing trend of X_c and T_m was observed with a decrease in x. When comparing the two SMPs with same x, the value of X_c of 4bxPCL-DTT and 4bxPCL-BPO was almost the same except for the sample with $x = 11$, while T_m of 4bxPCL-DTT was larger than that of 4bxPCL-BPO. Figure 3(c) shows the absolute value of DSC heat flow per unit mass $|j_H|$, proportional to specific heat of each SMP, at 300 K. The magnitude of j_H of 4bxPCL-BPO was larger than that of 4bxPCL-DTT and, in both 4bxPCL SMPs, the maximum $|j_H|$ was obtained in the sample with a minimum x (i.e., $x = 21$ for 4bxPCL-BPO and $x = 11$ for 4bxPCL-DTT).

3.2. Elastocaloric effect in 4bxPCL SMPs

In figure 4(a), we show the A and ϕ images of the 4b11PCL-DTT sheet at $\Delta\varepsilon = 1.5\%$ as an example of the result of the LIT measurement. The temperature modulation signal with uniform A and ϕ of $\sim 180^\circ$ was clearly observed in the sample. As shown in figure 4(b), the magnitudes of A and ϕ are independent of t_{int}, confirming the reversible temperature modulation during the LIT measurement. Figure 4(c) shows the $\Delta\varepsilon$ dependence of A and $\Delta\sigma$ for the 4b11PCL-DTT sheet. These linear relationships indicate that the elastocaloric effect obtained here is dominantly attributed to the mechanism (i), similar to the conventional plastic sheets [25]. In all of the samples used in this study, we obtained $\phi \sim 180^\circ$, indicating that heat is absorbed ($\Delta T < 0$) when stretching the sample. We confirmed the linear $\Delta\varepsilon$ dependence of A and $\Delta\sigma$ below $\Delta\varepsilon < 3\%$. To check endurance of the elastocaloric material, we performed repetitive LIT measurements in the 4b11PCL-DTT sheet. In figure 4(d), A and $\Delta\sigma$ at $\Delta\varepsilon = 2.0\%$ are plotted against the repetitive stretching number N_{rep} up to 10 000, where the LIT measurements with the accumulation time of 60 s and interval of 40 s were repeated by $N_{LIT} = 100$ times. The magnitudes of A and $\Delta\sigma$ were found to be independent of N_{rep}, confirming the durability of our elastocaloric material up to 10 000-repeated strains of 2.0%. Figure 4(e) depicts the relationship between $|\Delta T|$ and $\Delta\sigma$ at $\Delta\varepsilon = 1.0\%$ for the 4bxPCL SMP and plastic sheets. Since the data at upper (larger $|\Delta T|$) and left (smaller $\Delta\sigma$) positions in this graph correspond to higher performance of the elastocaloric temperature modulation, we found that 4bxPCL SMPs are better elastocaloric materials than the conventional plastics. Note that $|\Delta T|/\Delta\sigma$ of the PS sheet with $t = 1.0$ mm is 1.4×10^{-8} K Pa^{-1}, which is comparable to that of the PS sheets with $t = 0.2$ and 0.3 mm [25], showing that the difference in t is irrelevant to the present results. Figure 4(f) shows the x dependence of $|\Delta T|/\Delta\sigma$ for the 4bxPCL-BPO and -DTT samples. The $|\Delta T|/\Delta\sigma$ values of the PCL-based SMP sheets were larger than that of the HDPE sheet ($\sim 2.0 \times 10^{-8}$ K Pa^{-1}), the maximum among five conventional plastic sheets. In both SMP sheets, the values of $|\Delta T|/\Delta\sigma$ were almost the same in the range of $x \geqslant 32$, but below $x = 32$, the value of $|\Delta T|/\Delta\sigma$ increased with decreasing x. The maximum $|\Delta T|/\Delta\sigma$ observed here was estimated to be $\sim 3.0 \times 10^{-8}$ K Pa^{-1} in the 4b11PCL-DTT sheet, which leads to $\Delta S_{iso} \sim 7 \times 10^{-4}$ J g^{-1}K^{-1}. To compare the performance of elastocaloric materials, we can use the material-level dimensionless elastocaloric efficiency ζ [43, 44], defined as the ratio between the useful cooling/heating ($=\rho c_p|\Delta T|$) and the work input, i.e., the area between the $\Delta\sigma$-$\Delta\varepsilon$ curve and horizontal axis [13]: $\Delta\varepsilon\Delta\sigma/2$ in an elastic response. Here, we note that the material-level coefficient of performance COP_{mat} is also widely used for comparing elastocaloric materials but inappropriate for our samples; since the work input in COP_{mat} is defined by the area of the $\Delta\sigma$-$\Delta\varepsilon$ curve enclosed by loading and unloading curves ($=\oint\sigma d\varepsilon$), it is almost zero in the reversible elastic regime, leading to the divergence of COP_{mat}. Although the magnitude of $|\Delta T|$ and $|\Delta T|/\Delta\sigma$ of the PCL-based SMP sheets are still smaller than those of SMAs, ζ is estimated to be ~ 5 for our samples when $\rho = 1.1 \times 10^6$ g m^{-3} and $c_p = 1.8$ J g^{-1}K^{-1} are used [45, 46]. This ζ value is comparable to that of SMAs [13, 47]. Moreover, assuming that the 4b11PCL-DTT sheet is patterned into the same kirigami structure as shown in the PS sheets in [25] and the similar increase ratio of focused stress is obtained within the linear elastic response regime, the local $|\Delta T|/\Delta\sigma$ value will be enhanced around 4×10^{-7} K Pa^{-1}. This value is nearly an order of magnitude larger than that of SMAs, corresponding the local $|\Delta T|$ of over 1.0 K only at $\Delta\varepsilon = 2.0\%$ (note that the total $|\Delta T|/\Delta\sigma$ averaged over the kirigami-patterned sample is not enhanced).

Here, we discuss the origin of the x dependence of $|\Delta T|/\Delta\sigma$ in 4bxPCL SMPs. When we consider only the mechanism (i), equation (1) is simply reformulated as $|\Delta T_{ad}|/\Delta\sigma = |T_0\alpha/c|$, where α and c are the linear expansion coefficient and volumetric heat capacity, respectively [9]. According to the results of the DSC measurements (see section 3.1), c should increase with decreasing x. Thus, the dominant contribution of the enhancement of $|\Delta T|/\Delta\sigma$ with decreasing x is the increase in α. In the vicinity of T_m, the thermomechanical properties including α may be modulated as well as the mechanical properties [48, 49]. However, the decrease in T_m also causes the reduction of X_c and durability. The combination of small x and large X_c are crucial for enhancing $|\Delta T_{ad}|/\Delta\sigma$ at room temperature. Owing to the DTT cross-linking, the high rate of

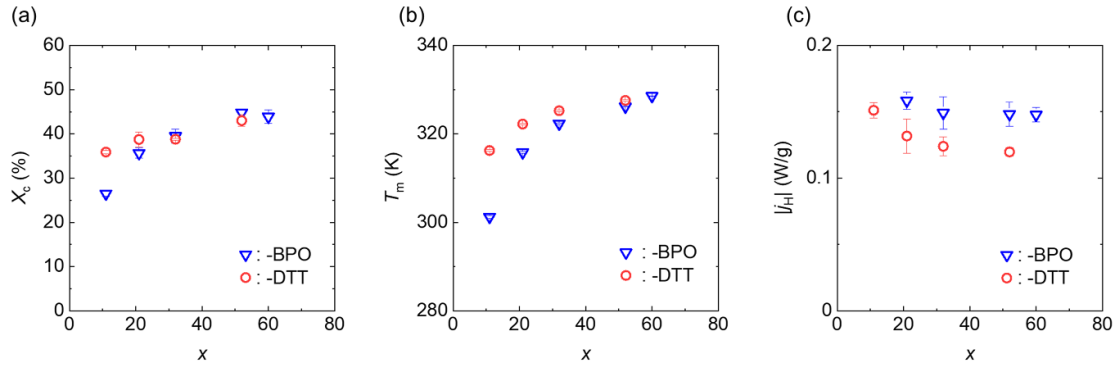

Figure 3. (a) x dependence of the crystallinity ratio X_c. (b) x dependence of the melting temperature T_m. (c) Absolute value of heat flow per unit mass $|j_H|$ at 300 K measured by differential scanning calorimetry for the 4bxPCL-BPO and 4bxPCL-DTT samples. In (c), the data for the 4b11PCL-BPO sample is absent because its T_m is close to room temperature.

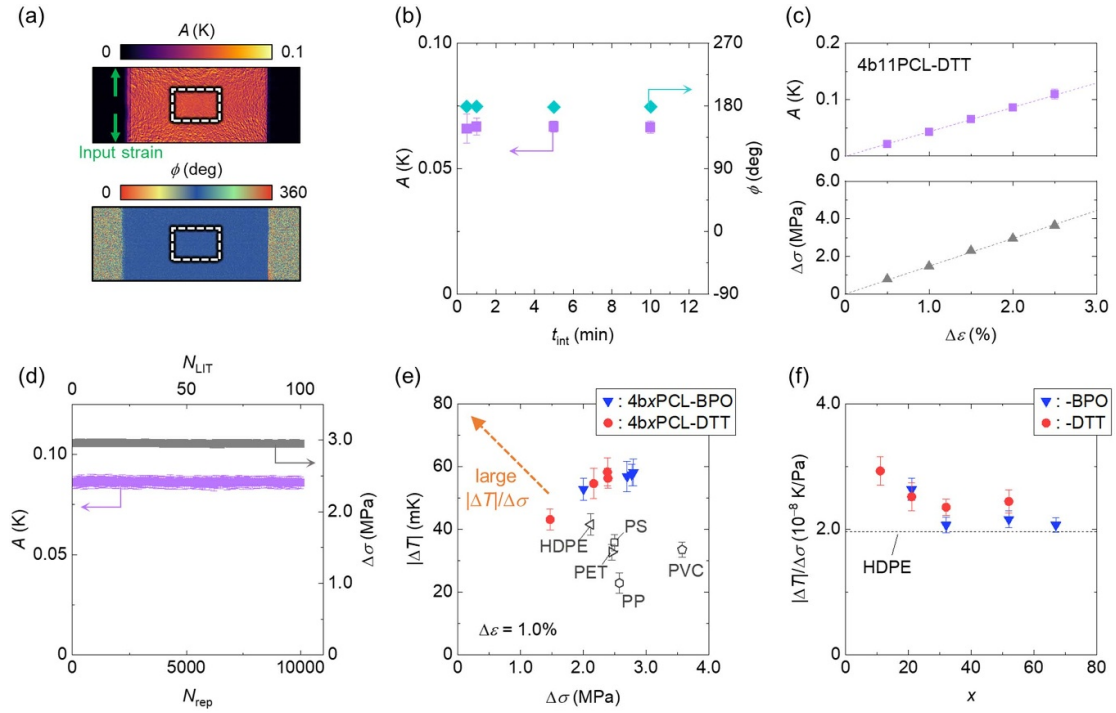

Figure 4. (a) A and ϕ images of the 4b11PCL-DTT sheet at $\Delta\varepsilon = 1.5\%$. Green arrows show the direction of the applied uniaxial strain. (b) Dependence of A and ϕ on the integration time of the LIT measurement t_{int} at $\Delta\varepsilon = 1.5\%$. The magnitude and error bars of the A and ϕ signals are the average and standard deviation of the data in the area surrounded by the white dashed rectangle in (a), respectively. (c) $\Delta\varepsilon$ dependence of A (upper panel) and $\Delta\sigma$ (lower panel) for the 4b11PCL-DTT sheet. (d) Stretching repetition number N_{rep} and LIT-measurement number N_{LIT} dependences of A and $\Delta\sigma$ for the 4b11PCL-DTT sheet at $\Delta\varepsilon = 2.0\%$. (e) Relation between the elastocaloric temperature modulation $|\Delta T| = |A\cos\phi|$ and $\Delta\sigma$ at $\Delta\varepsilon = 1.0\%$. In addition to the PCL-based SMP sheets, the data for the conventional plastic sheets including polystyrene (PS), polypropylene (PP), polyvinyl-chloride (PVC), high density polyethylene (HDPE), and polyethylene-terephthalate (PET) sheets with the thickness t of 1.0 mm are shown. The data for the 4b11PCL-BPO sample is absent because it is too fragile to measure the elastocaloric effect due to $T_m \sim$ room temperature. (f) Degree of polymerization x dependence of $|\Delta T|/\Delta\sigma$ for the 4bxPCL-BPO and -DTT sheets. The dotted line shows $|\Delta T|/\Delta\sigma$ for HDPE, which exhibit the maximum $|\Delta T|/\Delta\sigma$ value among the five conventional plastics.

ordered crystal structure can be kept even at room temperature in the 4bxPCL SMPs with small x, resulting in the large $|\Delta T_{ad}|/\Delta\sigma$.

3.3. Modulation of elastocaloric temperature change using shape memory effect

To further investigate the elastocaloric properties of SMPs, we performed the same measurements on the SMP sheets uniaxially deformed by the shape memory effect. Figure 5(a) shows the images of the PCL-based SMP sheets before and after deformation of which the procedure is as follows. First, the sheet clamped on the tensile machine was heated up to T_m using a blow-dryer. Then, while heating, the sheet was quickly stretched by a uniaxial deformation strain η, which was controlled by moving the clamps of the tensile machine.

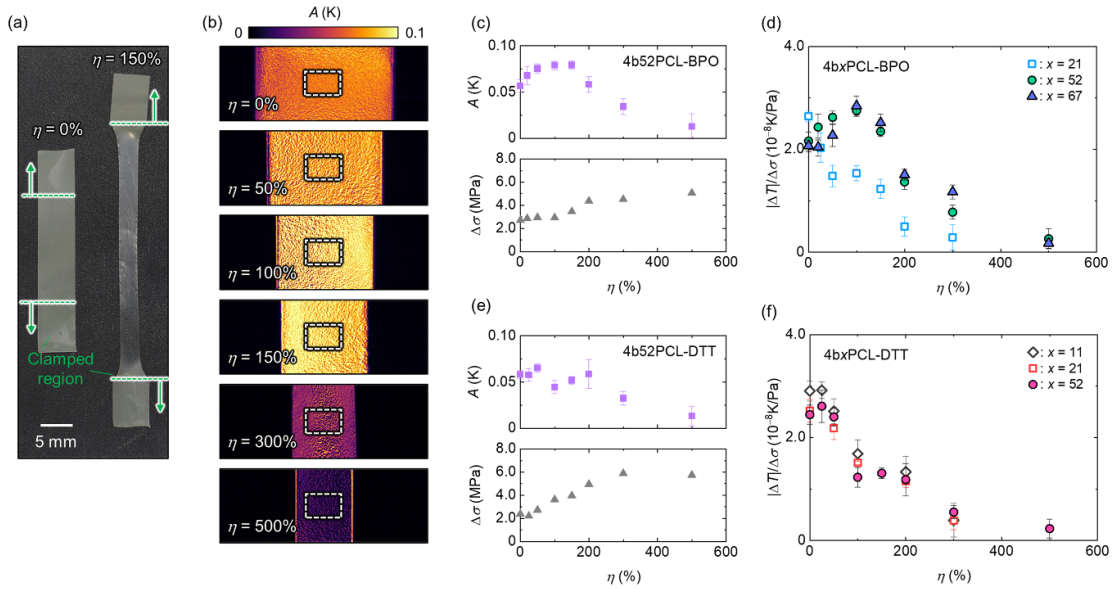

Figure 5. (a) Photograph of the 4b11PCL-DTT sheets before and after the deformation using the shape memory effect. η is the deformation strain. (b) A images of the 4b52PCL-BPO sheets at $\eta = 0\%$, 50%, 100%, 150%, 300%, and 500%. (c)[(e)] η dependence of A (upper panel) and $\Delta\sigma$ (lower panel) for the 4b52PCL-BPO (4b52PCL-DTT) sheet. The magnitude and error bar of A are the average and standard deviation of the data in the area surrounded by the white dashed rectangle in (b), respectively. (d)[(f)] η dependence of $|\Delta T|/\Delta\sigma$ for the 4bxPCL-BPO (4bxPCL-DTT) sheets for $x = 21$ (squares), 52 (circles), and 67 (triangles) [$x = 11$ (diamonds), 21 (squares), and 52 (circles)].

Finally, by cooling down the sheet to RT while holding the elongated sheet, the deformation was persistently fixed.

Figure 5(b) shows the A images of the 4b52PCL-BPO sheet at several η values. Even after the deformation, the distribution of the A signal in the SMP sheets is uniform. Importantly, the magnitude of the A signal depended on η. The upper panel of figure 5(c) shows the A signal as a function of η at $\Delta\varepsilon = 1.0\%$ in the 4b52PCL-BPO sheet. The magnitude of A was enhanced with increasing η below $\eta = 150\%$, where A at $\eta = 100\%$–150% were about 1.4 times larger than that at $\eta = 0\%$, but was decreased toward zero with further increasing η above 150%. However, the η dependence of $\Delta\sigma$ at $\Delta\varepsilon = 1.0\%$ was quite different from A: the clear increase in $\Delta\sigma$ was obtained only around $\eta = 150\%$ as shown in the bottom panel of figure 5(c). Such individual η dependences enhanced the $|\Delta T|/\Delta\sigma$ factor (light blue circle data points in figure 5(d)) to $\sim 3.0 \times 10^{-8}$ K Pa^{-1} at $\eta = 100\%$, a similar value obtained in the 4b11PCL-DTT sheet with $\eta = 0\%$. Although the enhancement of $|\Delta T|/\Delta\sigma$ around $\eta = 100\%$ was also observed in the 4b67PCL-BPO sheet, the $|\Delta T|/\Delta\sigma$ of the 4b21PCL-BPO sheet monotonically decreased with the increase in η (figure 5(d)). In the 4bxPCL-DTT samples, as shown in figures 5(e) and (f), the significant enhancement of A was not obtained and only the decrease in $|\Delta T|/\Delta\sigma$ with η increase was confirmed even in the sample with $x = 52$, whereas the $\Delta\sigma$-η relation showed the similar behavior.

Finally, we discuss the origin of the modulation of the elastocaloric properties induced by the shape memory effect. The dominant contribution is expected to be different from the mechanisms discussed in section 3.2, because uniaxial deformation via the shape memory effect induces the orientation of polymer chains and the change in the order from isotropic to anisotropic network with almost no change in crystallinity of PCL [50]. Previous reports show that the orientation of polymer chains monotonically reduces α in other polymers [51–53]. If this scenario is applicable to PCL-based SMPs, the dramatic reduction of A at large η can be explained, while the enhancement of A around $\eta = 100\%$–150% is still unclear. Thus, additional ΔS_{iso} induced by the mechanism (iii) corresponding to the conformation of polymer chains may exist. To clarify the microscopic mechanism and optimize $|\Delta T|/\Delta\sigma$ in SMPs, detailed analyses of their structures are necessary.

4. Conclusions

In conclusion, we investigated the elastocaloric effect of the PCL-based SMPs with two different cross-linking agents in the regime of the linear elastic deformation. By visualizing the elastocaloric temperature change using the LIT technique, we found that the elastocaloric performance, $|\Delta T|/\Delta\sigma$, in the PCL-based SMPs was higher than that in the conventional plastics and further enhanced by changing the cross-linking agent and

decreasing x. On the other hand, only in the PCL-based SMPs with BPO cross-linking and large x, the enhancement of $|\Delta T|/\Delta\sigma$ was demonstrated using the shape memory effect. These results reveal the potential of SMPs as elastocaloric materials and invigorate applications and materials science studies toward the realization of ultralow-stress-driven, flexible, and durable elastocaloric kirigami temperature modulators.

Data availability statement

All data that support the findings of this study are included within the article (and any supplementary files).

Acknowledgments

The authors thank R Yamamoto and Y Sasaki for technical supports. This work was partially supported by CREST 'Creation of Innovation Core Technologies for Nano-enabled Thermal Management' (No. JPMJCR17I1) and ERATO 'Magnetic Thermal Management Materials' (No. JPMJER2201) from JST, Japan; Grant-in-Aid for Transformative Research Areas(A) (No. JP20H05877) from JSPS, Japan; Innovative Science and Technology Initiative for Security (No. JPJ004596), ATLA, Japan; the Thermal and Electric Energy Technology Foundation; and the Canon Foundation.

ORCID iDs

Takamasa Hirai https://orcid.org/0000-0002-5577-8018
Koichiro Uto https://orcid.org/0000-0001-7091-0585
Mitsuhiro Ebara https://orcid.org/0000-0002-7906-0350
Ken-ichi Uchida https://orcid.org/0000-0001-7680-3051

References

[1] Moya X, Kar-Narayan S and Mathur N D 2014 Caloric materials near ferroic phase transitions *Nat. Mater.* **13** 439–50
[2] Wada H and Tanabe Y 2001 Giant magnetocaloric effect of $MnAs_{1-x}Sb_x$ *Appl. Phys. Lett.* **79** 3302–4
[3] Shen B G, Sun J R, Hu F X, Zhang H W and Cheng Z H 2009 Recent progress in exploring magnetocaloric materials *Adv. Mater.* **21** 4545–64
[4] Mischenko A S, Zhang Q, Scott J F, Whatmore R W and Mathur N D 2006 Giant electrocaloric effect in thin-film $PbZr_{0.95}Ti_{0.05}O_3$ *Science* **311** 1270–1
[5] Li B *et al* 2019 Colossal barocaloric effects in plastic crystals *Nature* **567** 506–10
[6] Mañosa L and Planes A 2017 Materials with giant mechanocaloric effects: cooling by strength *Adv. Mater.* **29** 1603607
[7] Kabirifar P, Trojer J, Brojan M and Tušek J 2022 From the elastocaloric effect towards an efficient thermodynamic, cycle *J. Phys. Energy* **4** 044009
[8] Goetzler W, Zogg R, Young J and Johnson C 2014 Alternatives to vapor-compression HVAC technology *ASHRAE J.* **56** 12–23
[9] Thomson W 1878 II. On the thermoelastic, thermomagnetic, and pyroelectric properties of matter *London, Edinburgh Dublin Phil. Mag. J. Sci.* **5** 4–27
[10] Chen H, Xiao F, Li Z, Jin X, Mañosa L and Planes A 2021 Elastocaloric effect with a broad temperature window and low energy loss in a nanograin Ti-44Ni-5Cu-1Al (at. %) shape memory alloy *Phys. Rev. Mater.* **5** 15201
[11] Chauhan A, Patel S and Vaish R 2015 Elastocaloric effect in ferroelectric ceramics *Appl. Phys. Lett.* **106** 172901
[12] Xie Z, Sebald G and Guyomar D 2016 Comparison of direct and indirect measurement of the elastocaloric effect in natural rubber *Appl. Phys. Lett.* **108** 041901
[13] Cui J, Wu Y, Muehlbauer J, Hwang Y, Radermacher R, Fackler S, Wuttig M and Takeuchi I 2012 Demonstration of high efficiency elastocaloric cooling with large ΔT using NiTi wires *Appl. Phys. Lett.* **101** 073904
[14] Ossmer H, Lambrecht F, Gültig M, Chluba C, Quandt E and Kohl M 2014 Evolution of temperature profiles in TiNi films for elastocaloric cooling *Acta Mater.* **81** 9–20
[15] Tušek J, Engelbrecht K, Mikkelsen L P and Pryds N 2015 Elastocaloric effect of Ni-Ti wire for application in a cooling device *J. Appl. Phys.* **117** 124901
[16] Tušek J, Engelbrecht K, Eriksen D, Dall'Olio S, Tušek J and Pryds N 2016 A regenerative elastocaloric heat pump *Nat. Energy* **1** 16134
[17] Bonnot E, Romero R, Mañosa L, Vives E and Planes A 2008 Elastocaloric effect associated with the martensitic transition in shape-memory alloys *Phys. Rev. Lett.* **100** 125901
[18] Vives E, Burrows S, Edwards R S, Dixon S, Mañosa L, Planes A and Romero R 2011 Temperature contour maps at the strain-induced martensitic transition of a Cu-Zn-Al shape-memory single crystal *Appl. Phys. Lett.* **98** 011902
[19] Mañosa L, Jarque-Farnos S, Vives E and Planes A 2013 Large temperature span and giant refrigerant capacity in elastocaloric Cu-Zn-Al shape memory alloys *Appl. Phys. Lett.* **103** 211904
[20] Lu B and Liu J 2017 Elastocaloric effect and superelastic stability in Ni-Mn-In-Co polycrystalline Heusler alloys: hysteresis and strain-rate effects *Sci. Rep.* **7** 2084
[21] Imran M and Zhang X 2020 Elastocaloric effects in polycrystalline Ni-Fe-Ga foams with hierarchical pore architecture *Phys. Rev. Mater.* **4** 065403
[22] Candau N, Chazeau L, Chenal J M, Gauthier C, Ferreira J, Munch E and Thiaudière D 2015 Strain induced crystallization and melting of natural rubber during dynamic cycles *Phys. Chem. Chem. Phys.* **17** 15331–8
[23] Xie Z, Wei C, Guyomar D and Sebald G 2016 Validity of Flory's model for describing equilibrium strain-induced crystallization (SIC) and thermal behavior in natural rubber *Polymer* **103** 41–45

[24] Xie Z, Sebald G and Guyomar D 2015 Elastocaloric effect dependence on pre-elongation in natural rubber *Appl. Phys. Lett.* **107** 081905
[25] Hirai T, Iguchi R, Miura A and Uchida K 2022 Elastocaloric kirigami temperature modulator *Adv. Funct. Mater.* **32** 2201116
[26] Lendlein A and Kelch S 2002 Shape-memory effect from permanent shape *Angew. Chem., Int. Ed.* **41** 2034–57
[27] Zarek M, Layani M, Cooperstein I, Sachyani E, Cohn D and Magdassi S 2016 3D printing of shape memory polymers for flexible electronic devices *Adv. Mater.* **28** 4449–54
[28] Lendlein A and Langer R 2002 Biodegradable, elastic shape-memory polymers for potential biomedical applications *Science* **296** 1673–6
[29] Bin H S, An Y and Yu W R 2019 Characterization and modeling of elastocaloric effects of shape memory poly(cyclooctene) *Appl. Phys. Lett.* **114** 013904
[30] Lendlein A, Schmidt A M and Langer R 2001 AB-polymer networks based on oligo(*ε*-caprolactone) segments showing shape-memory properties *Proc. Natl Acad. Sci.* **98** 842–7
[31] Ebara M, Uto K, Idota N, Hoffman J M and Aoyagi T 2012 Shape-memory surface with dynamically tunable nano-geometry activated by body heat *Adv. Mater.* **24** 273–8
[32] Uto K, Aoyagi T, DeForest C A, Hoffman A S and Ebara M 2017 A combinational effect of "bulk" and "surface" shape-memory transitions on the regulation of cell alignment *Adv. Healthcare Mater.* **6** 1601439
[33] Fulati A, Uto K, Iwanaga M, Watanabe M and Ebara M 2022 Smart shape-memory polymeric string for the contraction of blood vessels in fetal surgery of sacrococcygeal teratoma *Adv. Healthcare Mater.* **11** 2200050
[34] Uto K, Yamamoto K, Hirase S and Aoyagi T 2006 Temperature-responsive cross-linked poly(ε-caprolactone) membrane that functions near body temperature *J. Control. Release* **110** 408–13
[35] Lepoittevin B, Devalckenaere M, Pantoustier N, Alexandre M, Kubies D, Calberg C, Jérôme R and Dubois P 2002 Poly(ε-caprolactone)clay nanocomposites prepared by melt intercalation mechanical, thermal and rheological properties *Polymer* **43** 4017–23
[36] Fulati A, Uto K and Ebara M 2022 Influences of crystallinity and crosslinking density on the shape recovery force in poly(ε-caprolactone)-based shape-memory polymer blends *Polymers* **14** 4740
[37] Breitenstein O, Warta W and Langenkamp M 2010 *Lock-in Thermography: Basics and Use for Evaluating Electronic Devices and Materials* (Springer)
[38] Daimon S, Iguchi R, Hioki T, Saitoh E and Uchida K 2016 Thermal imaging of spin Peltier effect *Nat. Commun.* **7** 13754
[39] Hirayama Y, Iguchi R, Miao X F, Hono K and Uchida K 2017 High-throughput direct measurement of magnetocaloric effect based on lock-in thermography technique *Appl. Phys. Lett.* **111** 163901
[40] Uchida K, Daimon S, Iguchi R and Saitoh E 2018 Observation of anisotropic magneto-Peltier effect in nickel *Nature* **558** 95–99
[41] Modak R, Iguchi R, Sepehri-Amin H, Miura A and Uchida K 2020 Simultaneous direct measurements of conventional and inverse magnetocaloric effects in Ni-Mn-based Heusler alloys using lock-in thermography technique *AIP Adv.* **10** 065005
[42] Iguchi R, Fukuda D, Kano J, Teranishi T and Uchida K 2023 Direct measurement of electrocaloric effect based on multi-harmonic lock-in thermography *Appl. Phys. Lett.* **122** 082903
[43] Defay E, Crossley S, Kar-Narayan S, Moya X and Mathur N D 2013 The electrocaloric efficiency of ceramic and polymer films *Adv. Mater.* **25** 3337–42
[44] Moya X, Defay E, Heine V and Mathur N D 2015 Too cool to work *Nat. Phys.* **11** 202–5
[45] Gong T, Li W, Chen H, Wang L, Shao S and Zhou S 2012 Remotely actuated shape memory effect of electrospun composite nanofibers *Acta Biomater.* **8** 1248–59
[46] Suzuki Y, Duran H, Akram W, Steinhart M, Floudas G and Butt H J 2013 Multiple nucleation events and local dynamics of poly(ε-caprolactone) (PCL) confined to nanoporous alumina *Soft Matter* **9** 9189–98
[47] Qian S *et al* 2016 Elastocaloric effect in CuAlZn and CuAlMn shape memory alloys under compression *Phil. Trans. R. Soc.* A **374** 20150309
[48] Uto K, Ebara M and Aoyagi T 2014 Temperature-responsive poly(ε-caprolactone) cell culture platform with dynamically tunable nano-roughness and elasticity for control of myoblast morphology *Int. J. Mol. Sci.* **15** 1511–24
[49] Uto K, Aoyagi T, Deforest C A and Ebara M 2018 Dynamic alterations of hepatocellular function by on-demand elasticity and roughness modulation *Biomater. Sci.* **6** 1002–6
[50] Wang W, Jin Y, Ping P, Chen X, Jing X and Su Z 2010 Structure evolution in segmented poly(ester urethane) in shape-memory process *Macromolecules* **43** 2942–7
[51] Takeuchi Y, Shuto Y and Yamamoto F 1988 Band pattern development in shear-oriented thermotropic copolyester extrudates *Polymer* **29** 605–12
[52] Broer D J and Mol G N 1991 Anisotropic thermal expansion of densely cross-linked oriented polymer networks *Polym. Eng. Sci.* **31** 625–31
[53] Chen Y, Chen C, Rehman H U, Zheng X, Li H, Liu H and Hedenqvist M S 2020 Shape-memory polymeric artificial muscles: mechanisms, applications and challenges *Molecules* **25** 4246